Improvement of Slope Traversability for a Multi-DOF Tracked Vehicle with Active Reconfiguration of Its Joint Forms

Genki Yamauchi, Takahiro Noyori, Keiji Nagatani, and Kazuya Yoshida
School of Aerospace Engineering
Tohoku University
Aramaki-Aoba, Aoba-ku, Sendai, Japan
Email: yamauchi@astro.mech.tohoku.ac.jp

Abstract—During volcanic activity, people are restricted from coming within a certain distance to the volcano crater because of the danger posed. However, observing the restricted area is very important to reduce the risk to residents from eruptions such as pyroclastic and debris flows. Therefore, teleoperated mobile robots are being developed to observe conditions in such restricted areas, remotely. However, such volcanic environments include loose soil slopes of volcanic ash and lapillus, which may be impossible to traverse using current mobile robotics technology. Thus, we propose a contact angle control method for a multi-degrees of freedom (DOF) tracked vehicle. This controls the contact angle of the tracks and decreases the potential for the robot to sideslip on loose ground. To evaluate this method, we installed a contact load sensing system in each tracks. The effectiveness of the method was verified on an indoor simulated volcanic field and an outdoor field. In this paper, we explain the proposed method, introduce our developed robot and sensing system, and report the results of our evaluation experiments.

I. INTRODUCTION

Japan is a volcanic country with 110 active volcanoes in its domain. Once a volcano erupts, severe disasters can be caused by molten rock, ash, pyroclastic flows, and debris flows. Ensuring adequate warning of debris flows is an important task when planning an evacuation strategy to save residents in the area. To estimate the possibility of a debris flow, observing the piled ash on the volcano close to the crater is important. However, a restricted area is set around a volcano when it erupts for people's safety, e.g., 4 km from the crater in the case of a level 3 eruption at Mount Asama. Therefore, teleoperated robots are expected to observe such areas remotely.

Several volcano exploration robots have been developed, such as those by Robovolc [1], Dante I/II [2], and MOVE [3], and a number of experiments have been conducted in volcanic areas. These robots proved the usefulness of remote robotic observation. For instance, Dante II entered the Mount Spurr crater and surveyed the conditions of the volcano, remotely. However, the size and weight of the robot were very large, the observation was very complex, and the project ended in the 1990s.

To realize a **robotic remote observation system** for volcanic areas, we conducted field experiments with tracked vehicles [4][5] and a wheeled vehicle [6] at Mounts Asama, Aso, and Mihara. In these experiments, tracked vehicles prove high traversability, but some problems faced by them on steep

Fig. 1. Quince with flat lugs for volcano exploration: trying to traverse a weak slope on Mount Asama.

and weak slopes became clear. One of the biggest problems was the sideslip of the tracked vehicle, Quince, during lateral traversal on steep slopes (e.g., 30°), which prevented the robot from keeping to the given path. Figure 1 shows a snapshot of Quince traversing on a weak slope. Another big problem was the robot getting stuck during vertical traversal on a weak slope. Sometimes, slip prevention lugs mounted on the tracks dug into the ground, and the effective slope angle became larger than the actual one.

Several studies have examined slope traversal by mobile robots. Wettergreen et al. performed experiments that the sideslip of a wheeled robot can be reduced by changing the contact angle of the wheels [7]. Their Scarab robot had a mechanism to change the wheel height and thus the contact angle of the wheels. Inotsume et al. examined the primary factors for the sideslip of wheeled robots theoretically and experimentally and confirmed that the contact angle between the wheels and ground is the dominant factor [8]. These studies focused on wheeled rovers exploring extraterrestrial terrains such as the Moon and Mars. Thus, wheeled robots were selected because of their excellent traveling efficiency and simplified mechanisms. However, tracked robots generally

Fig. 2.   An overview of 11 D.O.F. tracked vehicle Elf

Fig. 3.   Illustration of slide mechanism for main tracks.

have much higher traversability than wheeled robots.

In our previous work, we developed an 11 degrees of freedom (DOF) tracked vehicle, called Elf [9]. Elf can change its contact angle to the ground by changing the joint angles of main tracks and sub-tracks, and we confirmed the effectiveness of this mechanism at reducing sideslip. In this study, we proposed an active reconfiguration method of the joint forms for a tracked vehicle to improve traversability on a weak slope. To evaluate this function, we developed a contact load measuring system using thin force sensing resistors (FSRs) in each track. In this paper, we explain the above control method, introduce our developed robot and sensing system, and report the results of our evaluation experiments.

II.   TARGET ROBOT

A. Overview

The target robot for our active reconfiguration method was the multi-DOF tracked vehicle Elf. Elf has two main tracks and four sub-tracks connected to each corner of the main track. It has eleven DOF: two for locomotion of the left and right tracks, two for each sub-track motion (for eight DOF), and one for the lifting slide mechanism between the main tracks. Figure 2 shows an overview of Elf.

In this study, the minimum version of Elf (i.e., two tracks) was used in an indoor experiment to verify the proposed control method because of size limitations. The full version of Elf (i.e., six tracks) was used in the outdoor field experiment. Flat grousers were fixed on the surface of the tracks with a height of 5 cm. Table I shows the specifications of Elf.

B. System characteristics

Elf has four sub-tracks; each sub-track contains actuators, batteries, a motor controller, and a wireless communication

TABLE I.   SPEC. OF ELF

Robot	
Dimensions	L1490(max) × W630 × H236 [mm]
Weight	48 [kg]
Main track	
Dimensions	L669 × W120 × H236 [mm]
Weight	48 [kg]
Sub-track	
Dimensions	L452 × W120 × H236 [mm]
Weight	6.6 [kg]
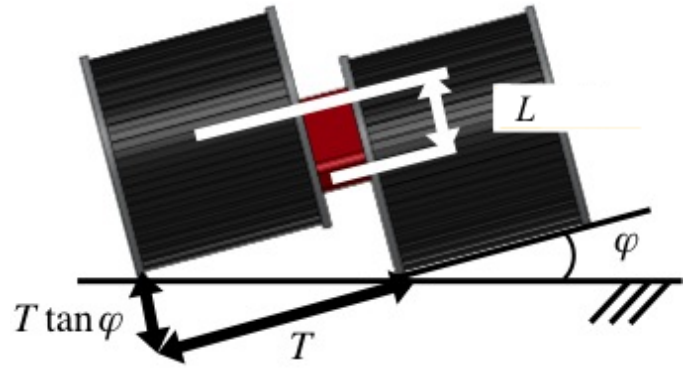
device (Xbee Wifi) that are all independent. All controllers communicate with an external laptop PC via wireless LAN (IEEEE802.11g).

C. Changing contact angle

The main body has two main tracks which are connected to a lifting slide mechanism that changes the contact angles of the tracks on the ground. Figure 3 shows the concept of the effect of this mechanism.

$$\phi = \tan^{-1}\left(\frac{L}{T}\right) \tag{1}$$

The maximum link length L_{max} and the tread T are 80 and 160 mm, respectively. Thus, Elf can change its contact angle from -25° to +25°.

Each sub-track is connected to one of the main tracks by a link with two actuated joints at both edges. The rotation of one joint permits only the wave motion of the sub-track, and the synchronized rotation of two joints permits a swinging motion of the sub-track while maintaining its attitude. The arm length A_{max} and the tread T are 80 and 160 mm, respectively. Thus, in the case of a swinging motion, Elf can change the contact angle of the sub-tracks from -25° to +25°.

III.   CONTACT LOAD MEASURING SYSTEM

A. Mechanism

To measure the ground reaction force on each track, thin force sensing resistors (FSRs) were installed in gaps between the belt guides and each track's body. Figure 4 shows the bottom of a sub-track without its belt. The two transparent bars are belt guides, and six FSRs were inserted under the guides in each sub-track, and sixteen FSRs were installed in each main track.

Figure 5 shows a conceptual illustration of the side view of the FSR layout. To detect the ground reaction force correctly and not to allow the guide to touch the body directly, a rubber sheet and pad were inserted between the sensor and belt guide. The sizes of the rubber sheet and pad were almost the same as the detecting area of the FSR. Bolts were used to fix the belt guide to the body with a liner bush and self-locking nut.
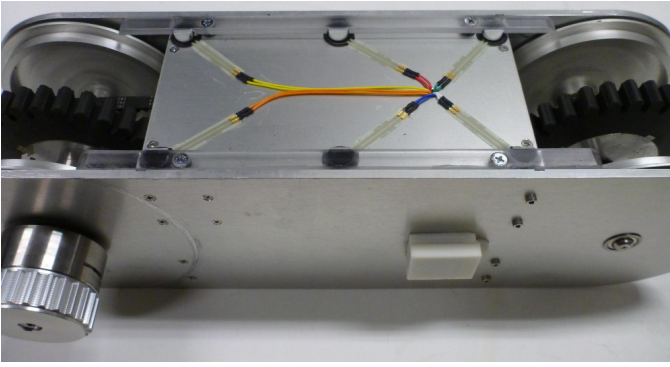
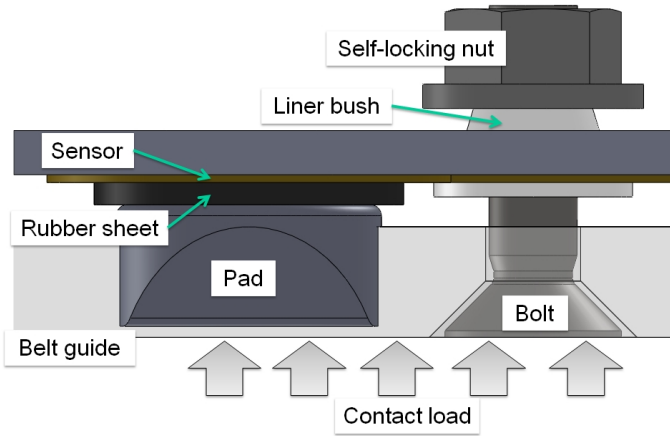Fig. 4. Contact load measurement system at bottom of sub-track without belt.

Fig. 5. Conceptual illustration of a side view of the FSR layout. The contact pressure is measured through the belt guides.

With the above mechanism, the FSR detects the normal contact force and prevents lateral force from the belt.

B. Basic performance evaluation test

To evaluate the system, we conducted a basic experiment using a single track on a rigid flat plane. The locomotion velocity was fixed to 10 cm/s, and sensor data were logged at 10 Hz.

Figure 6 shows the FSR data at the rear, center, front, and sum of them. The horizontal axis indicates the time, and the vertical axis indicates the detected force. The graph shows that the force detected by each sensor oscillated because of the discrete grousers on the track. A large force was detected when the grouser was located at the bottom of the sensor.

The sum of the FSR outputs indicated that the mass of the track was 6.0-8.1 kg for an average of 7.1 kg. The actual mass of the sub-track was about 6.6 kg. Therefore, the measurement errors were +23%, -9%, +8%, respectively. We suspect that the error was generated by the rotational motion of the tracks. The results show that the sensor cannot estimate the contact force distribution, but it is of practical use for detecting the mass of the tracks, roughly.
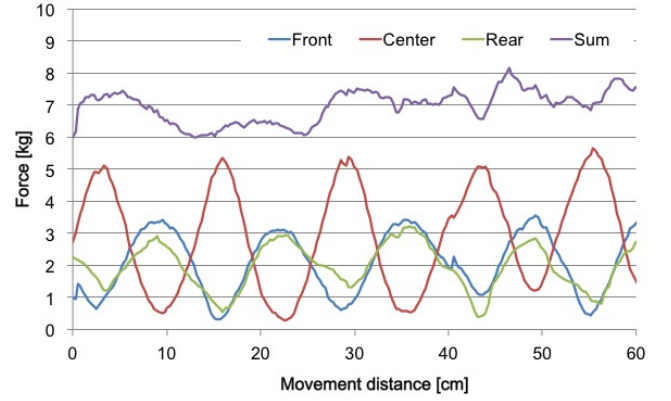

Fig. 6. Experimental results of forces vs. movement distance

IV. SLOPE TRAVERSAL OF MULTI-DOF TRACKED VEHICLE

When a mobile robot traverses a weak slope, a sideslip is generated downhill because of (1) the collapse of the weak ground and (2) slippage on the surface. To prevent the above situations and improve the traversability of the robot, we propose a control method (given below) for the contact surface of tracks on weak ground.

A. Lateral force model

The slope angle α is expressed by the following equation:

$$\alpha = \theta_{roll} + \varphi, \qquad (2)$$

where the contact angle between the bottom of the track and the slope surface is φ and the roll angle is θ_{roll}.

When the bottoms of tracks are parallel to the ground, as shown in Figure 7, the contact angle φ is zero. On the other hand, when the robot changes its configuration of tracks, the normal force $\sum_{i=1}^{2} Fy_i$ and the lateral force $\sum_{i=1}^{2} Fz_i$ are respectively expressed as follows:

$$\sum_{i=1}^{2} Fy_i = W \sin(\alpha - \varphi), \qquad (3)$$

$$\sum_{i=1}^{2} Fz_i = W \cos(\alpha - \varphi) \qquad (4)$$

where the gravity force is expressed as W.

According to the above equations, the lateral force $\sum_{i=1}^{2} Fy_i$ increases with the slope angle α. On the other hand, when the contact angle φ is equal to the slope angle α, the lateral force is minimized, which should reduce the sideslip caused by slippage on the surface of the slope.

B. Contact force model

Figure 7 shows the vertical forces of the left track F_1 and the right track F_2, which are calculated geometrically by the
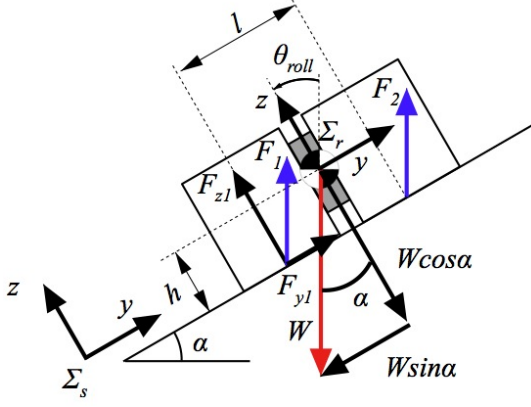
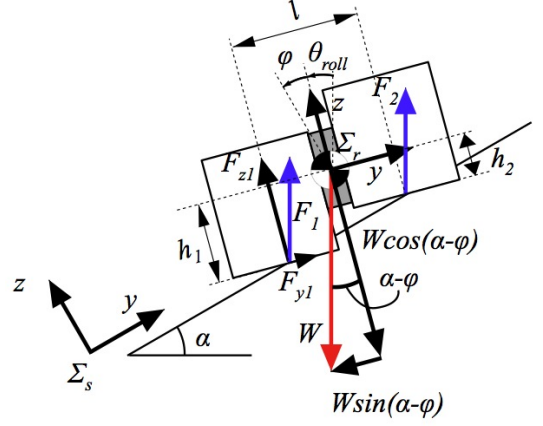Fig. 7. Forces acting on a tracked vehicle under normal contact configuration.

Fig. 8. Forces acting on a tracked vehicle under leveled contact configuration.

following equations:

$$F_1 = \frac{W}{2} + \frac{h}{l}W\tan\alpha \qquad (5)$$

$$F_2 = \frac{W}{2} - \frac{h}{l}W\tan\alpha \qquad (6)$$

where h is the distance between the height of the center of gravity and l is the tread of tracks. According to the equations, a larger slope angle α means a larger bias for both contact forces.

On the other hand, when the robot changes the contact angle φ, the contact force also changes, as shown in Figure 8. The the vertical forces of the left track F_1 and right track F_2 can be calculated geometrically by the following equations:

$$F_1 = \frac{W\left(\frac{l\cos(\alpha-\phi)}{2} + h_1\sin(\alpha-\phi)\right)}{l\cos(\alpha-\phi) + (h_1 - h_2)\sin(\alpha-\phi)} \qquad (7)$$

$$F_2 = \frac{W\left(\frac{l\cos(\alpha-\phi)}{2} - h_2\sin(\alpha-\phi)\right)}{l\cos(\alpha-\phi) + (h_1 - h_2)\sin(\alpha-\phi)}. \qquad (8)$$

According to the above equations, when the contact angle φ is equal to the slope angle α, the contact force of each track is equalized as follows:

$$F_1 = F_2 = \frac{W}{2}. \qquad (9)$$

C. Contact angle control method

As noted earlier, sideslip can be reduced by changing the contact angle of the tracks. In particular, when the contact angle φ is equal to the slope angle α, the contact force of each track is equalized, and the possibility of the collapse of weak ground can be minimized.

To realize the above motion, we propose a control method that equalizes the contact angle with the slope angle. The reference of the contact angle φ_{ref} is derived from the

relationship between the roll angle of the robot θ_{roll} and the current contact angle $\varphi_{current}$ as follows:

$$\varphi_{ref} = \alpha$$
$$= \theta_{roll} + \varphi_{current} \qquad (10)$$

where the roll angle θ_{roll} is obtained by an Inertial Measurement Unit (IMU) on the robot and the contact angle $\varphi_{current}$ is calculated from the Eq. (1).

To maintain the contact angle $\varphi_{current}$ at the calculated value, we implemented a PID controller on the robot.

V. Experiments

A. Indoor experiment

To confirm the effectiveness of the proposed control method, we conducted an experiment on an indoor weak slope field. The field was 3 m in length and 1 m in width; it was filled with pumice stones. Figure 9 shows an overview of the field.

In this experiment, we set the slope angle from 15° deg to 30° in increments of 5°. The minimum version of Elf (two tracks) was used because of the size limitations of the field. The velocity of the robot was set to 8 cm/s.

In order to evaluate the traversability of the robot, we used the slip angle β. This is the angle between the desired and the actual trajectories and is expressed by

$$\beta = \tan^{-1}\left(\frac{l_y}{l_x}\right) \qquad (11)$$

where l_x is the desired direction and l_y is the actual movement.

When a robot traverses a slope, the sideslip and the change in orientation of the robot (yaw angle) both generate its lateral movement. To eliminate the effect of the orientation error, we adopted the following orientation control:

$$v_l = v + c\theta_{yaw} \qquad (12)$$
$$v_r = v - c\theta_{yaw}, \qquad (13)$$

where v is the reference velocity, θ_{yaw} is the orientation of the robot obtained by the mounted IMU, c is the coefficient

Fig. 9. Simulated volcanic field. The field was filled with pumice stones, and the slope angle was set manually.

Fig. 10. Slip angles at different slope angles:(red) without proposed control method and (blue) with proposed control method, at each slope angle.

value, and v_l and v_r are the velocities of the left and right tracks, respectively, that are obtained by encoders attached to the motors.

In order to evaluate the effectiveness of the control method at equalizing the vertical forces on the left and right tracks, the contact load measuring system presented in section III was used in this experiment.

The experimental results are shown in Figure 10, which graphs the relationship between the slope and the slip angles. The slip angle increases with the slope angle, but the slip angle is reduced by an average of 67% with the proposed method.

Figure 11 shows the resulting changes in the contact force difference when the slope angle was 20°. These results were obtained by the contact load measuring system. According to Eqs. 5 and 6, the difference was 0.0 kgf with the proposed control and 6.6 kgf without the control. In the results, the average difference was 2.2 kgf with the proposed control and 6.0 kgf without the control. The proposed control method could not realize a difference of zero, but the results were improved by 63% on average.

The above results simply presents the effectiveness of the proposed method.

B. Outdoor experiment

In the indoor experiment, only the main tracks were employed because of the limited width of the test field. To confirm the applicability of the control method to the full-sized Elf including sub-tracks, we conducted a field experiment in an open space for testing construction equipment at the Public Works Research Institute, in Japan. The field was 5 m in length and 3 m in width with a slope of about 20°.

As described in the section IV-C, the reference contact angle φ_{ref} was derived from the link length and track tread. For sub-tracks, the length between the main track and sub-track was the same as the tread between the main tracks. Therefore, the same control method can be applied to the sub-tracks by
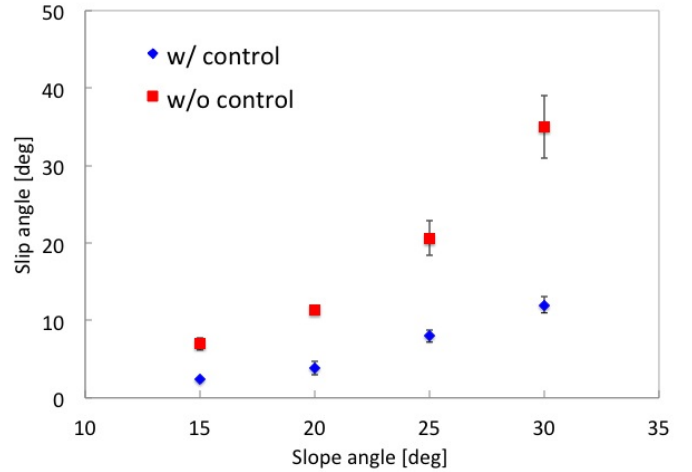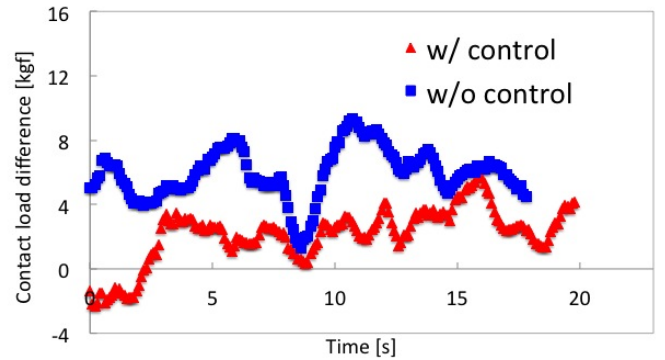

Fig. 11. Differences in contact forces between left and right tracks when slope angle = 20°: (red) with proposed method and (blue) without proposed method.

controlling their height using two actuated joints to maintain the track's attitude.

The experimental scene is shown in Figure 12, and the resulting slip angles are shown in Figure 13. The graph includes the results of the indoor experiment (when the slope angle was 20°) that were given in the previous section.

The slip angle was improved by about 12% using the proposed control method. This is a small improvement but not significant. We considered this to be due to the following reasons.

In this experiment, the slope was not soft, and the tracks did not become sufficiently buried. The slope was made of loamy soil from the Kanto district, and it rained before the experiment. Therefore, even if the surface of the field was deformable, the slope was rigid. Thus, the grousers did not dig into the soil enough, and tracks could not be formed, as shown in Figure 8. Therefore, the improvement in the outdoor experiment was limited.
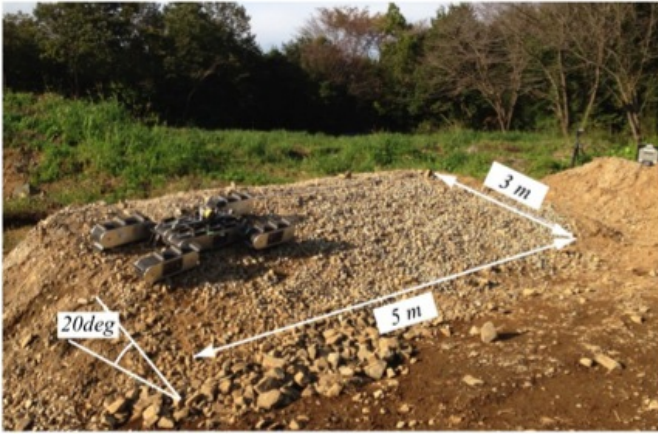
Fig. 12. Outdoor field for experiment. The field was made of loamy soil from the Kanto district. The slope was covered with crushed stone.
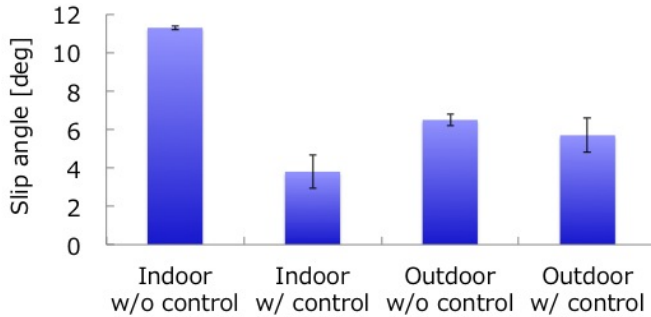

Fig. 13. Summary of experimental results for slope angle = 20°.

VI. CONCLUSION AND FUTURE WORKS

We introduced the multi-DOF tracked vehicle Elf and its contact load measuring system. Furthermore, we proposed a contact angle control method for Elf when traversing slopes laterally. The effectiveness of the method was verified by indoor experiments on the slip angle.

In the outdoor experiment, the improvement was limited because of the rigid field conditions. For actual volcanic fields, the surface is much softer, and the control method should work well in such a weak environment. Future work will involve confirming our expectations in an actual volcanic environment.

In this study, we assumed that the slope is flat. In actual situations, the target environment is uneven terrain. Therefore, to improve the traversability of the tracked vehicle in such an environment, we need to consider an adaptive control of the sub-tracks that adjusts to the roughness of the surface. To realize such intelligent motion, we need to obtain three-dimensional terrain information and adaptive control of the sub-tracks. This will be very challenging and important future work.

ACKNOWLEDGMENT

REFERENCES

[1] G. Muscato, D. Caltabiano, S. Guccione, et al., "ROBOVOLC: A Robot for volcano exploration ? Result of first test campaign", Industrial Robot : An International Journal, Vol. 30, N.3,pp.231-242, 2003.

[2] John E. Bares, David S. Wettergreen, "Dante II: Technical Description, Results, and Lessons Learned", International Jounal of Robotics Research, vol. 18 no. 7 621-649, 1999.

[3] Akihiko Yokoo, Mie Ichihara, Akio Goto, Hiromitsu Taniguchi, "Atmospheric pressure waves in the field of volcanology', *Shock Waves*,vol. 15, Issue 5 , pp 295-300, 2006.

[4] Eric Rohmer, Tomoaki Yoshida, Kazunori 0hno, Keiji Nagatani, Satoshi Tadokoro, Eiji Koyanagi, "Quince: A Collaborative Mobile Robotic Platform for Rescue Robots Research and Development", *International Conference on Advanced Mechatronics*, pp.225-230, 2010.

[5] Keiji Nagatani, Hiroaki Kinoshita, Kazuya Yoshida, Kenjiro Tadakuma, Eiji Koyanagi, "Development of leg-track hybrid locomotion to traverse loose slopes and irregular terrain", *Journal of Field Robotics*,Volume 28, Issue 6, pp.950-960, 2011.

[6] Keiji Nagatani,Ken Akiyama,Genki Yamauchi,Hikaru Otsuka,Takuma Nakamura,Seiga Kiribayashi,Kazuya Yoshida,Yasushi Hada,Shini'chi Yuta,Kenichi Fujino,Tomoyuki Izu,Randy Mackay, "Volcanic Ash Observation in Active Volcano Areas using Teleoperated Mobile Robots –Introduction to Our Robotic-Volcano-Observation Project and Field Experiments–", *Proceedings of the 2013 IEEE Int'l Workshop on Safety, Security and Rescue Robotics*, pp.21-26, 2013.

[7] David Wettergreen, Scott Jared Moreland, Krzysztof Skonieczny, Dominic Jonak, David Kohanbash, and James Teza, "Design and field experimentation of a prototype Lunar prospector", International Journal of Robotics Research, Vol. 29, No. 12, pp. 1550 - 1564, 2010.

[8] Hiroaki Inotsume, Masataku Sutoh, Kenji Nagaoka, Keiji Nagatani, and Kazuya Yoshida, "Evaluation of the Reconfiguration Effects of Planetary Rovers on their Lateral Traversing of Sandy Slopes", *IEEE International Conference on Robotics and Automation*, pp.3413-3418, 2012.

[9] Keiji Nagatani,Takahiro Noyori, and Kazuya Yoshida, "Development of Multi-D.O.F. Tracked Vehicle to Traverse Weak Slope and Climb up Rough Slope", *IEEE/RSJ International Conference on Intelligent Robots and Systems*, pp. 2849-2854, 2013.